On a new coordinate system for improved discrimination of vegetation and burned areas using MIR/NIR information

Renata Libonati [a,c,*], Carlos C. DaCamara [a], José Miguel C. Pereira [b], Leonardo F. Peres [d]

[a] University of Lisbon, IDL/CGUL, Lisbon, Portugal
[b] School of Agriculture, Technical University of Lisbon, Lisbon, Portugal
[c] Center for Weather Forecast and Climate Studies, Brazilian National Institute for Space Research, Cachoeira Paulista, Brazil
[d] Federal University of Rio de Janeiro, Rio de Janeiro, Brazil

ARTICLE INFO

ABSTRACT

A transformation defined on the near-infrared (NIR) and middle-infrared (MIR) space is presented that allows deriving a new coordinate system appropriate for vegetation and burned area discrimination. The transformation is based on the difference between MIR and NIR in conjunction with the distance from a convergence point in the MIR/NIR space, representative of a totally burnt surface. One of the derived coordinates presents a small scatter for pixels associated to vegetated surfaces (strict scale) whereas the other one covers a wide range of values (large scale) that suggest its use as a proxy of water content of vegetation. The strict scale character of the first coordinate together with the large scale character of the second one make the coordinate system especially adequate to discriminate vegetated surfaces and rank them according to the water content, from green and dry to burned vegetation. The performance of the new coordinate system is then assessed against than traditional ratio or modified ratio indices (namely the Vegetation Index, the Burned Area Index and the Global Environmental Monitoring Index, modified to the MIR/NIR space) and it is shown that the new coordinate system provides better information than traditional indices, opening interesting perspectives for burned area discrimination and other applications like drought monitoring.

© 2011 Elsevier Inc. All rights reserved.

1. Introduction

Over the last decades, several studies have demonstrated the effectiveness of the reflectance of middle-infrared (MIR) for discriminating among different types of vegetation (Holben and Shimabukuro, 1993; Shimabukuro et al., 1994; Kaufman and Remer, 1994; Goita et al., 1997); estimating total and leaf biomass of several forest ecosystems (Boyd et al., 1999; 2000); and monitoring intra- and inter-annual climate-induced changes in vegetation (Boyd and Duane, 2001; Boyd et al., 2002). MIR reflectance has also proven to be useful when applied to burned area discrimination (e.g. Roy et al., 1999; Barbosa et al., 1999; Pereira, 1999). It may be nevertheless noted that, when used to identify vegetation and detect its changes, the MIR band is commonly used together with the near-infrared (NIR), given the strong contrast between the two bands, green vegetation displaying high reflectance in the latter and low reflectance in the former. In fact, vegetation reflectance in the NIR, around 0.8 μm, is affected primarily by leaf structure (Slaton et al., 2001); green vegetation exhibits high reflectance values but, after the leaf matures, the cells enlarge, crowd together, reducing the intercellular space and leading to a decrease in reflectance (Gates et al., 1965). On the other hand, MIR is often employed as a surrogate of the traditional red (R) band (around 0.6 μm), based on the fact that MIR reflectance is well correlated to the R one, but is not sensitive to most aerosols, namely to those associated with smoke from biomass burning events (Libonati et al., 2010). Kaufman and Remer (1994) showed that the correlation between MIR and R is due to the simultaneous occurrence of processes that darken the surface in these two bands. Whereas in the visible wavelengths, the pigmentation of leaves, especially by active chlorophyll, absorbs the solar radiation, reducing the reflectivity, in the MIR domain (around 3.5 - 3.9 μm) the cellular water content, present in green vegetation, causes a strong absorption, reducing the reflectance at these wavelengths (Gates et al., 1965; Salisbury and D'Aria, 1994). As green leaves become senescent due to the decrease of the levels of chlorophyll and water content, the absorption of solar radiation drops off in both R and MIR regions, increasing reflectance at the two bands.

Within the framework of the above described context, substantial efforts have been spent by the research community in the development of vegetation indices (Verstraete and Pinty, 1996). For instance, the development of optimal vegetation indices in the R/NIR spectral domain has greatly benefited from the so-called soil line concept (Rondeaux et al., 1996). Introduced by Richardson and Wiegand (1977), the soil line concept is a linear relationship between NIR and R reflectances of bare soil, where changes in soil reflectance are

* Corresponding author at: University of Lisbon, IDL/CGUL, Lisbon, Portugal.
  E-mail address: rlsantos@fc.ul.pt (R. Libonati).

associated to moisture and organic matter (Baret et al., 1993), and departures from the soil line are in turn strongly related to biophysical parameters such as the Fraction of Green Vegetation, FGV, or the Fraction of Absorbed Photosynthetically Active Radiation, FAPAR (Pinty and Verstraete, 1992). The soil line is therefore a constraint in the R/NIR spectral space that greatly contributes to the design of new vegetation indices that are insensitive to the soil background while remaining responsive to vegetation (Pinty et al., 2008). Examples of improved alternatives to the traditional Normalized Difference Vegetation Index, NDVI (Rouse et al., 1973) are the Perpendicular Vegetation Index, PVI (Richardson and Wiegand, 1977), the Soil-Adjusted Vegetation Index, SAVI (Huete, 1988) and the Global Environment Monitoring Index, GEMI (Pinty and Verstraete, 1992).

However, to the best of our knowledge, no similar constraint has been found in the MIR/NIR space, a circumstance that may have impaired the design of optimal vegetation indices, which have been heuristically derived from indices already developed in the R/NIR domain. This is the case of VI3 (Kaufman and Remer, 1994), a modification of NDVI, as well as of GEMI3 (Pereira, 1999) that directly resulted from GEMI. As pointed out by the developers of VI3 and GEMI3, the derivation of the indices was primarily based on the fact that MIR and R reflectance are strongly correlated. On the other hand, as also stressed by the authors, the processes that govern reflectance in R and MIR are not expected to lead to similar results and the existence of other processes that may change reflectance in the two channels cannot be ignored.

The aim of the present paper is to investigate the possibility of defining a transformation in the MIR/NIR space that leads to an enhancement of the spectral information about vegetation. For this purpose, and taking into account the methodology suggested by Verstraete and Pinty (1996) to design optimal indices, a new space is proposed and an appropriate coordinate system is then defined that is suitable to discriminate vegetation and is sensitive to its water content. The rationale adopted may be viewed as comparable to that followed to derive the tasseled cap transformation (Crist and Cicone, 1984; Kauth and Thomas, 1976; Cohen et al., 1995), where a new coordinate system is introduced in order to optimize data for vegetation studies. Using satellite imagery, it will be then shown that the proposed coordinate system is particularly appropriate to

operationally monitor vegetation and to detect vegetation changes, in particular those caused by droughts and fire events.

Accordingly, the three specific goals of the present study may be stated as follows:

1. To study the possibility of defining a transformation in the MIR/NIR space leading to an enhancement of the spectral information about vegetation;
2. To define a new coordinate system representing an improved combination of the MIR and NIR channels when the two spectral bands are used to detect vegetation changes, in particular those caused by droughts and fire events;
3. To assess the added value brought by the proposed coordinate system when applied to real satellite data.

2. Data

The present study relies on data from remotely-sensed observations, as well as from laboratory measurements. Remotely-sensed observations were gathered over two main Brazilian biomes, namely the Amazon Forest and the Cerrado region (see Fig. 1 and Table 1) as covered by 16 Landsat ETM + images. Data consist of top of the atmosphere (TOA) values of MIR radiance, NIR reflectance and thermal infrared (TIR) brightness temperature, acquired by the Moderate Resolution Imaging Spectrometer (MODIS) instrument on-board Terra satellite during the year of 2002, together with the respective solar zenith angles. Data were obtained from the Terra/MODIS Level 1B 1 km V5 product, MOD021 (MCST, 2006) and correspond to channels 2 (centered at 0.858 μm), 20 (centered at 3.785 μm), and 31 (centered at 11.017 μm). Surface values of MIR reflectance were then retrieved by applying the methodology developed by Kaufman and Remer (1994), paying special attention to the possible drawbacks previously pointed out by Libonati et al. (2010).

Validation of results from the analysis performed on MODIS images was mainly carried out based on ETM + imagery. Direct validation of results in the MIR domain is, however, a difficult task because of the lack of "in-situ" (direct) measurements of MIR reflectance. This limitation may be partially circumvented by laboratory measurements
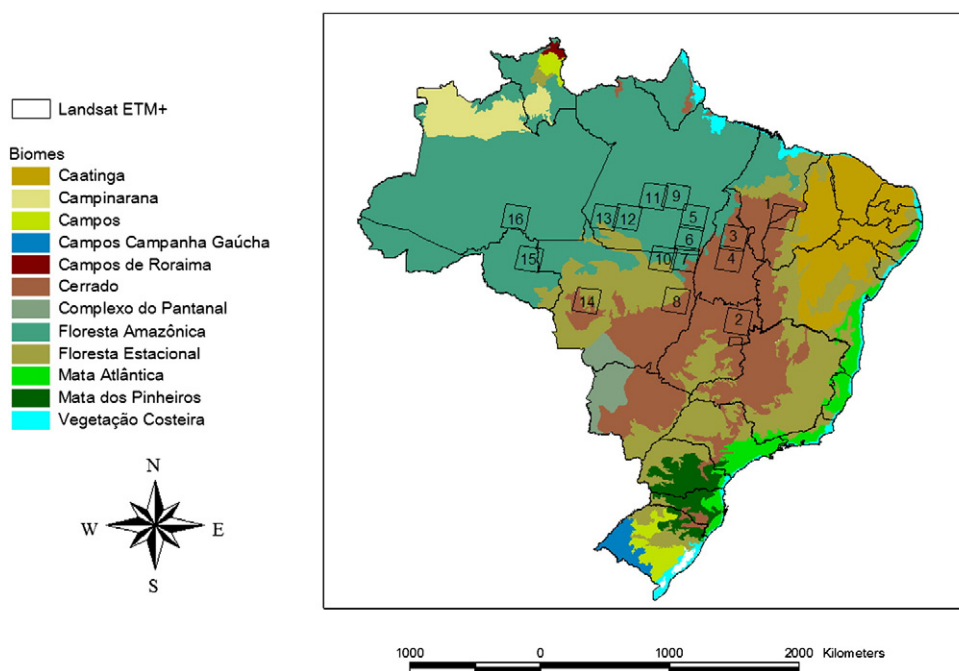

Fig. 1. Map of Brazil showing IBAMA's classification of general biomes. Numbered frames provide the location of the 16 Landsat ETM + scenes (as listed in Table 1).

Table 1
List of 16 Landsat ETM + images, acquisition dates, locations and biomes covered.

TM scene number	Path/row	Date (mm/dd/yyyy)	Location	Biome
1	220/65	06/28/2002	Maranhão/Piauí	Cerrado
2	221/70	06/05/2002	Goiás	Cerrado
3	222/66	08/15/2002	Tocantins	Cerrado
4	222/67	08/15/2002	Tocantins	Cerrado
5	224/65	08/13/2002	Pará	Amazon Forest
6	224/66	08/13/2002	Pará	Amazon Forest
7	224/67	08/13/2002	Mato Grosso	Cerrado/ Amazon Forest
8	224/69	08/29/2002	Mato Grosso	Cerrado/ Deciduous Forest
9	225/64	08/20/2002	Pará	Amazon Forest
10	225/67	08/04/2002	Mato Grosso	Amazon Forest/ Deciduous Forest
11	226/64	08/11/2002	Mato Grosso	Cerrado/ Deciduous Forest
12	227/65	08/18/2002	Pará	Amazon Forest
13	228/65	08/09/2002	Pará	Amazon Forest
14	228/69	10/28/2002	Pará	Amazon Forest
15	231/67	06/11/2002	Rondonia	Amazon Forest
16	232/65	08/05/2002	Amazonas	Amazon Forest

of MIR reflectance. In this respect, spectral libraries are currently available that may provide useful information about the spectral features and ranges of the reflectance for natural and manmade materials. Spectral libraries are, in fact, commonly used as reference sources for the identification of surfaces in remote sensing imagery, but the spectral range currently covered differs from library to library. For instance, the MODIS University of California-Santa Barbara (UCSB) spectral library provides information in TIR domain (from 3 to 14 μm), whereas the Advanced Spaceborne Thermal Emission and Reflection Radiometer (ASTER) spectral library (Baldridge et al., 2009) makes available spectral reflectance data from the visible to the TIR domains (from 0.4 to 15.4 μm). The analysis was restricted to materials belonging to vegetation, water, and soil classes from the ASTER spectral library because of data accessibility constraints in both NIR and MIR regions. Spectral libraries like ASTER and MODIS/UCSB supply reliable reflectance data for different types of materials, such as vegetation, water, soil, rocks and manmade materials. However, to the best of our knowledge, no reflectance measurements are currently available for charcoal, ash or any burned plant material, in the spectral region accounted for in this study (MIR region). Therefore, four fire residue samples were collected at Alta Floresta, state of Mato Grosso, Brazil. The samples were collected and kindly made available by the Combustion Laboratory from INPE (LCP/INPE). Fire residues were also collected by J.M.C.P. in Portugal from samples of burned maritime pine trees. Charcoal samples (from both Brazil and Portugal) were sent to

the NASA Jet Propulsion Laboratory, where spectral signatures were measured.

For each laboratory spectral data described above, the MODIS channel equivalent reflectance was computed by convolving the laboratory spectral reflectance signatures with the MODIS channels normalized response function. Fig. 2 depicts the computed reflectance values in MODIS channels 2 and 20 for different samples from the ASTER spectral library, as well as from the burned material samples.

Finally, for the sake of simplicity, MODIS channels 1, 2 and 20 will be hereafter referred to as R, NIR and MIR, respectively.

3. Methods

3.1. Rationale

The distribution, over the MIR/NIR space, of a variety of classes of materials obtained from laboratory measurements are shown in Fig. 2 (left panel). It may be noted that the different materials tend to form clusters on the MIR/NIR space and that there is an overall displacement along the diagonal of the graph, from vegetation (top left corner), down to burned materials (bottom right corner) across the soil surfaces. The same behavior may be observed in Fig. 2 (right panel), which presents segments connecting the locations of pre- and post-fire mean values of MIR and NIR reflectance. These segments, the so-called displacement vectors respect to 12 burned scars in MODIS
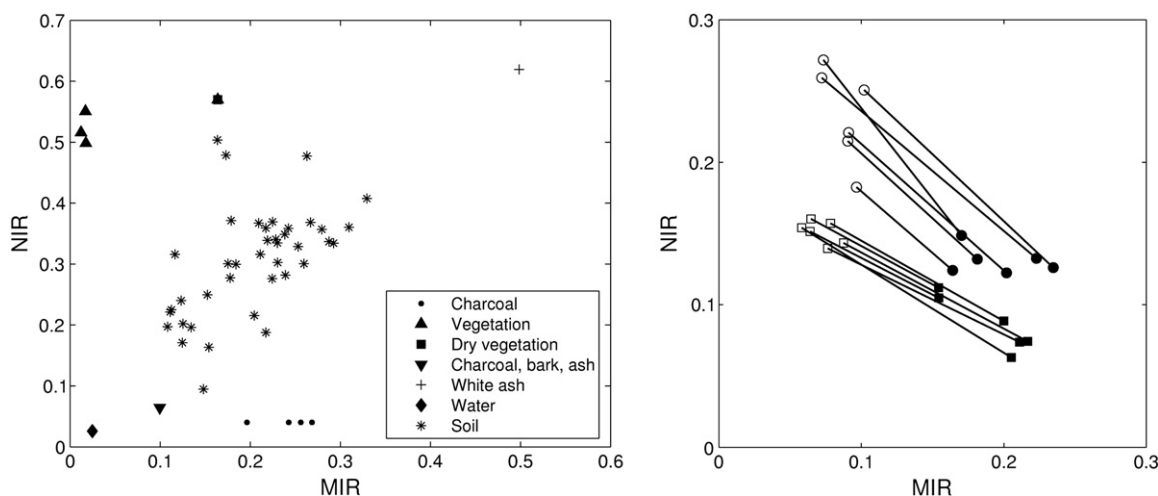

Fig. 2. Left panel: Scatter plot in the MIR/NIR spectral domain for different classes of materials obtained from laboratory measurements. Right panel: Pre-fire (open symbols) and post-fire (black symbols) mean values of MIR and NIR over 12 selected scars in the Amazon (circles) and Cerrado (squares). Displacement vectors in the MIR/NIR spectral domain are represented by solid lines.

images, six of them over the Amazon and the remaining six over Cerrado. The identification of recent burned pixels in MODIS images was based on burned area polygons, as derived from visual classification of Landsat ETM + images (Table 1). Changes of reflectance from pre- to post-fire are indicated by line segments. Results obtained from both laboratory and imagery data provide an indication that the radiative signatures of vegetation and burned surfaces may be adequately discriminated in the MIR/NIR space by means of appropriate spectral indices.

For instance, aiming at the identification of dark, dense vegetation, Kaufman and Remer (1994) proposed a new vegetation index, the so-called VI3, which is a modified version of the traditional NDVI, the R reflectance being simply replaced by the reflective part of the MIR signal (channel 3 from AVHRR sensor). VI3 was heuristically derived from NDVI taking into account the fact that MIR reflectance tends to correlate well with R reflectance. The insensitivity of MIR to atmospheric effects, namely to aerosols associated to burning biomass, together with the characteristics of MIR that make this spectral region especially appropriate to distinguishing between burned and unburned surfaces led Pereira (1999) to suggest applying VI3 for mapping burned scars according to the following formula:

$$VI3 = \begin{cases} \dfrac{(\rho_{NIR} - \rho_{MIR})}{(\rho_{NIR} + \rho_{MIR})}, & \text{for } \rho_{NIR} \geq \rho_{RED} \\ 0, & \text{for } \rho_{NIR} < \rho_{RED} \end{cases} \tag{1}$$

where ρ_{MIR} and ρ_{RED} are the MIR and red reflectance, respectively. The restriction $\rho_{NIR} \geq \rho_{RED}$ prevents the index from being erroneously applied to water surfaces where it is ill defined (Kaufman and Remer, 1994).

Pereira (1999) also considered the possibility of adapting GEMI for mapping fire-affected areas. Defined in the R/NIR space originally proposed by Pinty and Verstraete (1992), GEMI is an optimized vegetation index designed to minimize contamination of the vegetation signal by extraneous factors, such as the atmosphere and the soil background. GEMI was modified by replacing AVHRR channel 1 (R) by channel 3 (MIR) leading to the so-called GEMI3:

$$GEMI3 = \frac{\Theta(1 - 0.25\Theta) - (\rho_{MIR} - 0.125)}{1 - \rho_{MIR}} \tag{2}$$

where:

$$\Theta = \frac{2\left(\rho_{NIR}^2 - \rho_{MIR}^2\right) + 1.5\rho_{NIR} + 0.5\rho_{MIR}}{\rho_{NIR} + \rho_{MIR} + 0.5} \tag{3}$$

A similar procedure may be applied to modify the so-called Burned Area Index (BAI), which was specifically designed for burned area discrimination in AVHRR R/NIR imagery over Mediterranean environments (Martín, 1998). BAI is defined as the inverse spectral distance to a previously fixed convergence point, given by the minimum (maximum) reflectance of burned vegetation in the NIR (R) bands. The corresponding index in the AVHRR MIR/NIR space may be heuristically defined as:

$$BAI3 = \frac{1}{(\rho_{NIR} - \rho_{CNIR})^2 + (\rho_{MIR} - \rho_{CMIR})^2} \tag{4}$$

where ρ_{CNIR} and ρ_{CMIR} are the coordinates of the above-mentioned convergence point, given by the NIR minimum and MIR maximum values of reflectance for burned vegetation (see Fig. 3 for an example using MODIS). Although to the best of our knowledge BAI has never been modified using the MIR channel, reasonable results were found when replacing R by the shortwave infrared (SWIR) region, which presents spectral response to fire scars similar to that observed in the MIR region.
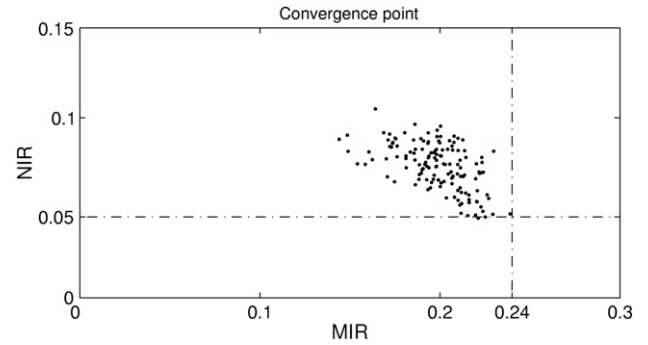

Fig. 3. MIR and NIR reflectance bi-spectral space showing the reflectance convergence point of recently burned areas samples as extracted from 12 burned scars in MODIS images covering the north, northwest and midwest of Brazil, six of them over the Amazon and the remaining six over Cerrado. Dashed-dot lines delimit the upper and lower bounds in MIR and NIR and their intersection is the convergence point.

All three modified indices described above have proven to be useful in burned area detection in many regions of the world. However it is worth recalling that those indices were obtained in a heuristic way from corresponding ones defined in the R/NIR space and that the original indices were in turn affected by several shortcomings. For instance, as pointed out by Martín and Chuvieco (2001), the original BAI index strongly depends on the soil background, the atmospheric conditions, and geometry of illumination and observation. This is due to the non-ratioing concept behind BAI as opposed to NDVI and GEMI where ratioing reduces many forms of noise (e.g. illumination differences, cloud shadows, atmospheric attenuation) that are present in multiple bands. In the case of GEMI it is its nonlinear behaviour that makes the index an effective cloud detector (Briggs and Mounsey, 1989) due to the high reflectance of clouds in R and it is to be expected that GEMI3 may perform likewise for burns, which are the most reflective surfaces in MIR channel after cloud-screening of the study area. However the coefficients of GEMI were kept unchanged in GEMI3 formulation, which may not reproduce the desired sensitivity to burned events in some cases. The same can be argued in the case of VI3 that keeps the same coefficients as NDVI.

Taking into account the above referred limitations, there is room for improvement in the design of improved indices to discriminate burned areas in the MIR/NIR spectral domain. One may start by noting that besides the ratioing concept there is another structural feature that distinguishes VI3 and GEMI3 from BAI3. Whereas the first two indices involve differences between NIR and MIR channels, BAI3 is based on distances in the MIR/NIR space from a pre-defined fixed point. An assessment of the roles played by differences between MIR and NIR channels and distances in the MIR/NIR space may be performed by looking at the behavior of the following two indices defined within the context of the MODIS MIR/NIR space:

$$\eta = \sqrt{(x - x_0)^2 + (y - y_0)^2} \tag{5a}$$

$$\xi = x - y \tag{5b}$$

where x and y are the reflectance of MODIS NIR and MIR channels, and x_0 and y_0 are the respective reflectances of the convergence point. It is worth noting that index ξ may be viewed as a modified Difference Vegetation Index (Richardson and Wiegand, 1977) where the slope of the soil line is set to unity and where the R channel is replaced by MIR. Taking into account the range of observed values of MIR (NIR) reflectance in burned surfaces (Fig. 3) the value of 0.24 (0.05) was prescribed to $x_0 (y_0)$ as the upper (lower) bound of MIR (NIR). Choice of values for x_0 and y_0 is also supported by the fact that the set of

laboratory measurements of burned samples (Fig. 2) presents lower MIR (higher NIR) values than x_0 (y_0).

A quantitative assessment of the performance of η and ξ was performed by evaluating the potential of the two indices to discriminate between vegetation and burned scars. The assessment is based on a discrimination index similar to the one proposed by Kaufman and Remer (1994), i.e.

$$M = \frac{|\mu_v - \mu_b|}{(\sigma_v - \sigma_b)} \tag{6}$$

where μ_v (μ_b) is the mean value for vegetation (burned scars) and σ_v (σ_b) is the standard deviation for the vegetation (burned scars). M may be viewed as an estimator of signal-to-noise ratio, the absolute difference between the mean values of the two classes representing the signal (associated to between-group variability) and the sum of the standard deviations representing noise (associated to within-group variability). Values of M larger than one indicate good separability, whereas values smaller than one represent large degrees of histogram overlap between the two classes.

A set of 255 burned pixels was therefore selected from Landsat ETM + scenes 3, 4 6 and 8 (Table 1), together with a set of 343 pixels associated to vegetation and values of the discriminating index M were computed for indices η and ξ.as well as for VI20, GEMI20 and BAI20, respectively obtained from NDVI, GEMI and BAI by replacing the R band (MODIS channel 1) by the MIR band (MODIS channel 20). As shown in Table 2 indices η and ξ are very similar in what respects to their ability to discriminate between vegetation and burned surfaces and the performance of both indices is very similar to the ones of VI20 and GEMI20 and significantly better than the performance of BAI20. It may be therefore concluded that despite their formal simplicity the proposed indices η and ξ are both appropriate to burned area discrimination.

This may be further verified by superimposing the contour lines of ξ and η (Fig. 4) over the displacement vectors associated to pre- and post fire values of MIR and NIR reflectance. As pointed out by Verstraete and Pinty (1996), the more perpendicular a displacement vector is to the contour lines of a given index, the better the sensitivity of the index to the observed change at the surface. Despite the small sample size, it seems that η is especially sensitive to burning events in the Amazon forest, whereas ξ is more appropriated in Cerrado. Following Liang (2004), the two indices will be compared in a single plot and an analysis will be made of the η/ξ space.

3.2. The η/ξ space

Let U be the unit square in the MIR/NIR space and let U' be the corresponding image in the η/ξ space by means of the transformation defined by Eqs. (5a) and (5b). The domains U and U' are shown in Fig. 5, together with a set of selected points in U and the respective images in U'. Because of its shape, the domain U' will be hereafter referred to as the kite domain.

Let A(x_0,y_0) be the convergence point so that A'(0, x_0-y_0) is the corresponding image according to the transformation given by Eqs. (5a) and (5b). The curve [A'B'C'] ([A'F'E']) that defines the

Table 2
Discriminating ability between vegetation and burned surfaces (M index) respecting to proposed indices η and ξas well as to VI20, GEMI20 and BAI20 for Landsat ETM + scenes 3, 4, 6 and 8 (Table 1) over the Amazon and Cerrado regions.

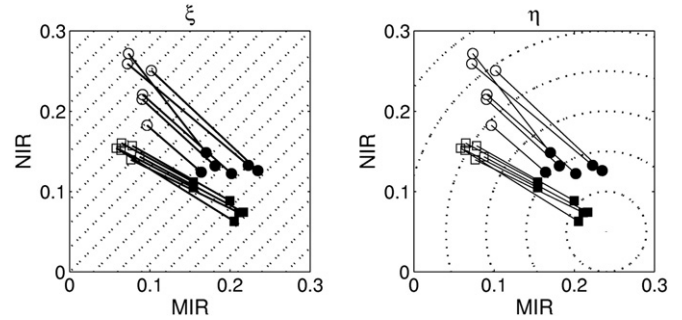| Index	M
η	3.33
ξ	3.27
VI20	3.31
GEMI20	3.21
BAI20	1.11

Fig. 4. As in Fig. 2 (right panel) but with contours (dotted lines) of ξ (left panel) and η (right panel) superimposed on displacement vectors (solid lines).

upper (lower) limit of U' will be the set of points that, for each value of $\xi \geq x_0 - y_0$ ($\xi \leq x_0 - y_0$), have the minimum value of η. The respective equations of the curves may accordingly be obtained by replacing Eq. (5b) into Eq. (5a) and then solving $\left(\frac{\partial \eta}{\partial x}\right)_\xi = 0$, leading to:

$$2x - (x_0 + y_0 + \xi) = 0. \tag{7}$$

Replacing Eq. (5b) into Eq. (7) leads in turn to:

$$y = -x + (x_0 + y_0). \tag{8}$$

Given the limits of U, the straight line defined by Eq. (8) will go from point B(x_0+y_0, 0) to point F(0, x_0+y_0). The image of segment $\overline{BF}$ may therefore be obtained by replacing Eq. (8) into Eq. (5b) leading to

$$\eta = \frac{|\xi - (x_0 - y_0)|}{\sqrt{2}} \tag{9}$$

i.e., to:

$$\eta = \begin{cases} -\dfrac{\xi - (x_0 - y_0)}{\sqrt{2}}, & \xi \in [-(x_0 + y_0), x_0 - y_0] \\ \dfrac{\xi - (x_0 - y_0)}{\sqrt{2}}, & \xi \in [x_0 - y_0, x_0 + y_0] \end{cases}. \tag{10}$$

It may be noted that the straight line with positive slope goes from A'(0, x_0-y_0) to B'($\sqrt{2}y_0$, x_0+y_0), whereas the straight line with negative slope goes from F'($\sqrt{2}x_0$, -(x_0+y_0)) to A'(0, x_0-y_0). Beyond point B (point F), the minimum distances to point A, for a given value of ξ, will be located along segment $\overline{BC}$ (segment $\overline{FE}$). Since $\overline{BC} = \{(x,0), x \in [x_0 + y_0, 1]\}$, then $\xi = x$ along the respective image and, taking Eq. (5a) into account, η will be given by:

$$\eta = \sqrt{(\xi - x_0)^2 + y_0^2}, \xi \in [x_0 + y_0, 1] \tag{11}$$

In an analogous way, $\xi = -y$ along the image of $\overline{FE} = \{(0,y), y \in [x_0 + y_0, 1]\}$ and therefore:

$$\eta = \sqrt{x_0^2 + (\xi + y_0)^2}, \xi \in [-1, -(x_0 + y_0)] \tag{12}$$

D(1,1) is the point in domain U with maximum value of ξ and its image, D'$\left(\sqrt{(1-x_0)^2 + (1-y_0)^2}, 0\right)$, is readily obtained by means of Eqs. (5a) and (5b).

The right limits of the kite domain U' are defined by the images of segments $\overline{ED} = \{(x,1), x \in [0,1]\}$ and $\overline{CD} = \{(1,y), y \in [0,1]\}$. Taking into account that $x = 1 + \xi$ along $\overline{ED}$, the respective image will be given by:

$$\eta = \sqrt{(1 + \xi - x_0)^2 + (1 - y_0)^2}, \xi \in [-1, 0] \tag{13a}$$
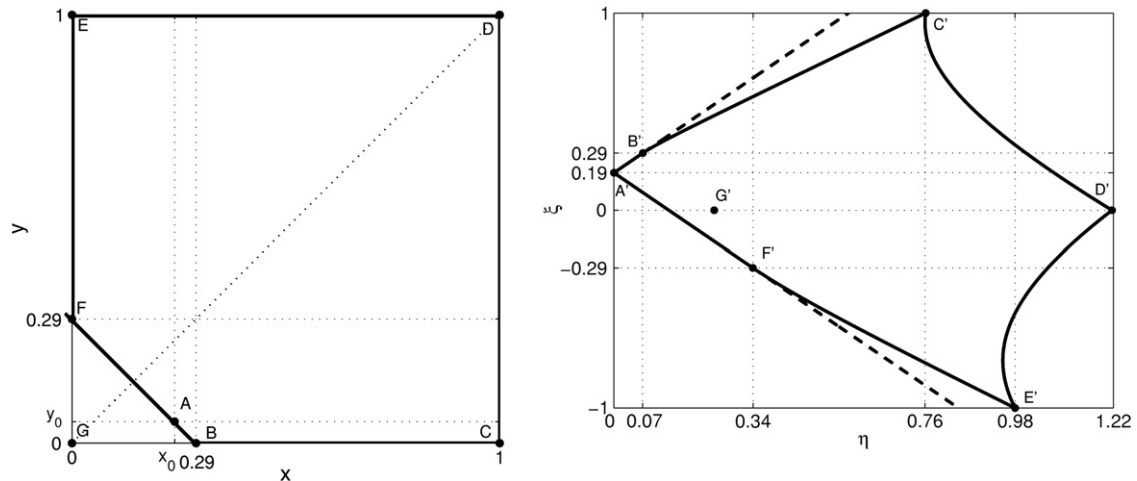
Fig. 5. The unit square U in the x-y space and the kite domain U' in the η/ξ space, together with a set of selected points in U and the respective images in the kite domain U'.

The image of $\overline{CD}$ may be finally obtained in a similar way by noting that $y = 1 - \xi$ along the segment, leading to:

$$\eta = \sqrt{(1-x_0)^2 + (1-\xi-y_0)^2}, \ \xi \in [0,1] \tag{13b}$$

Table 3 presents the coordinates (x,y) of all above considered points as well as the coordinates (η,ξ) of the respective images.

For further reference, the inverse forms of Eqs (10)–(13) are given below.

Top boundary [A'B'C']

$$\xi = \begin{cases} \sqrt{2}\eta + (x_0-y_0), & 0 \le \eta \le \sqrt{2}y_0 \\ \sqrt{\eta^2-y_0^2} + x_0, & \sqrt{2}y_0 \le \eta \le \sqrt{(1-x_0)^2 + y_0^2} \end{cases} . \tag{14}$$

Bottom boundary [A'F'E']

$$\xi = \begin{cases} -\sqrt{2}\eta + (x_0-y_0), & 0 \le \eta \le \sqrt{2}x_0 \\ -\sqrt{\eta^2-x_0^2} - y_0, & \sqrt{2}x_0 \le \eta \le \sqrt{x_0^2 + (1-y_0)^2} \end{cases} . \tag{15}$$

Fig. 6 is a plot in space η/ξ of the points shown in Fig. 2. It may be noted that the materials corresponding to vegetation and charcoal, as well as part of the samples corresponding to soil tend to lie along the bottom boundary line, as given by Eq. (15). On the other hand, three samples of charcoal lie along the top boundary line, as defined by Eq. (14). As shown in Fig. 7, a similar behavior may be observed with the pixels of mean pre- and post-fire reflectance values from the 12

selected scars (Fig. 2, right panel), which all lie along the bottom boundary line of the kite domain. This consistent behavior strongly suggests defining an adequate coordinate system in space η/ξ.

3.3. The V-W coordinate system

The kite domain U' being limited, and taking into account the fact that vegetated surfaces (green or burned) tend to lie along the top and bottom boundaries of U', it is advantageous to define a system of coordinates (V, W) such that the boundaries of the domain (Fig. 5, right panel) are coordinate curves, e.g. V remaining constant along [A'B'C'] as well as along [A'F'E'], and W being constant along [C'D'E']. Fig. 8 presents such coordinate system whose analytical derivation over the kite domain U' may be found in the Appendix. As shown in Fig. 9, the coordinate system (V, W) may be viewed as defining a spider web over the original unit square U in the MIR/NIR space.

Fig. 10 (left panel) presents the coordinates V and W of the laboratory measurements shown in Fig. 6, but with discrimination among the different types of soil. It is worth noting that vegetation samples and some soil types containing organic matter (e.g. Inceptisol, Mollisol, Entisol and Alfisol) are in close alignment with the coordinate curve V = 1 On the other hand, dry vegetation, water, charcoal and the remaining soil types, in particular Aridisol, do not lie
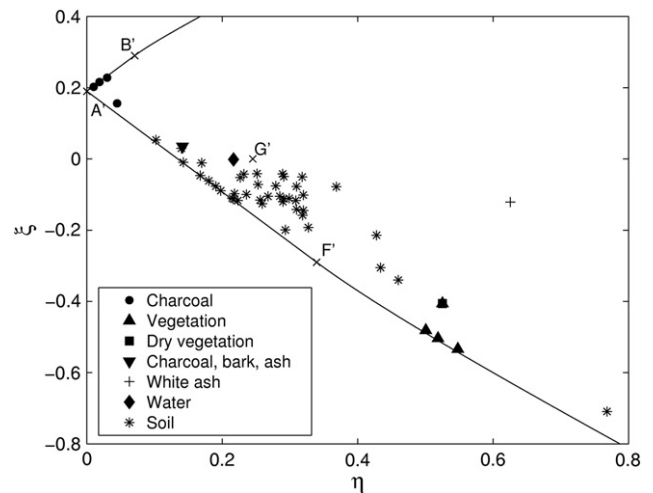
Table 3
Coordinates (x,y) of the considered points in Fig. 5 (left panel) and coordinates (η,ξ) of the respective images (right panel).

	U domain			U' domain	
	x	y		η	ξ
A	x_0	y_0	**A'**	0	x_0-y_0
B	x_0+y_0	0	**B'**	$\sqrt{2}y_0$	x_0+y_0
C	1	0	**C'**	$\sqrt{(1-x_0)^2 + y_0^2}$	1
D	1	1	**D'**	$\sqrt{(1-x_0)^2 + (1-.y_0)^2}$	0
E	0	1	**E'**	$\sqrt{x_0^2 + (1-y_0)^2}$	-1
F	0	x_0+y_0	**F'**	$\sqrt{2}x_0$	$-(x_0+y_0)$
G	0	0	**G'**	$\sqrt{x_0^2 + y_0^2}$	0

Fig. 6. Location in space η/ξ of laboratory measurements respecting to five types of materials.
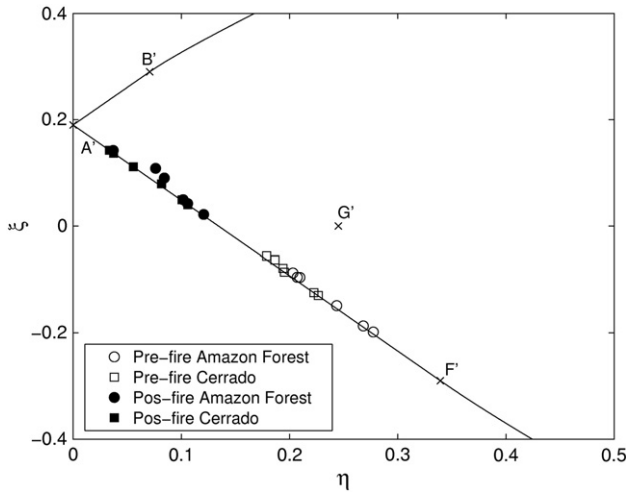
Fig. 7. Images in space η/ξ of the points shown in Fig. 2 (right panel).

Fig. 9. The spider web system of coordinates (V, W) in the unit square U of the original MIR/NIR space. Contour lines of V from −1 to 1 (with intervals of 0.2) and contour lines of W from 0 to 1 (with intervals of 0.1). The spider web system of coordinates was obtained by successively applying Eqs. (5a) and (5b) to the original unit square U in the MIR/NIR space and then by applying Eqs. (A5) and (A7).

near V = 1. In fact, Aridisols, which never fall close to V = 1, are the dominant soil types in deserts and xeric shrublands, and have a very low concentration of organic matter. A less stable behavior may be observed for the other soil types; for instance Mollisols, which tend to have high organic matter content, fall close to V = 1 in the case of the Cryoboroll sub-class but the same does not happen with the other sub-classes. This may be attributed to the fact that the overall soil reflectance is controlled by carbonate and quartz rather than by organic matter (Salisbury and D'Aria, 1994). It is also worth pointing out that, besides tending to lie along the contour line V = 1, surfaces of green and burned vegetation as well as soils containing organic matter tend to organize themselves according to water content, with green vegetation, soils and burned vegetation being respectively associated to large (~ 0.6),moderate (~ 0.2-0.4) and low values (~ 0) of W. Fig. 10 (right panel) presents the V-W coordinate system in the more familiar MIR/NIR space, which defines a "spider-web" whose cells are associated to the different types of surfaces.

The above-described behavior of vegetated surfaces according to water content is confirmed by the results shown in Fig. 11 corresponding to the V and W coordinates of the pre- and post-fire samples shown in Figs. 4 and 7. All surfaces of green and burned vegetation are accordingly located along coordinate curve V = 1, pre-
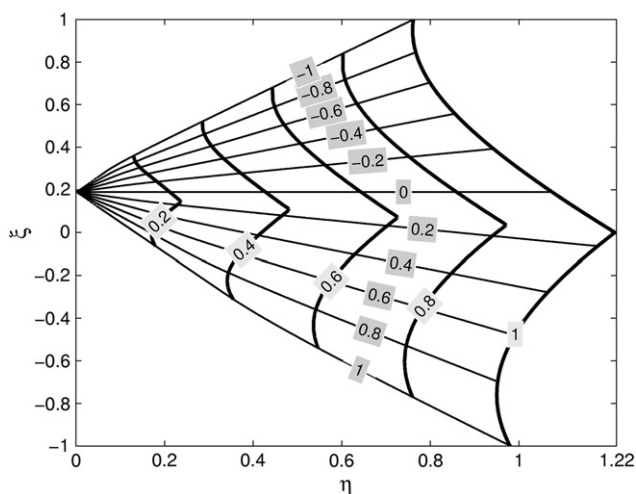
fire (post-fire) pixels, with green, dry and burned vegetation being associated to decreasing values of W.

Finally, it is worth emphasizing that V and W present very different properties regarding the scatter of values; whereas coordinate V has a very small scatter for pixels associated with green, dry and burned vegetation, coordinate W covers a much wider range of values. As pointed out by Verstraete and Pinty (1996), the complementary character of coordinates V and W is especially appropriate for application purposes since the strict scale character of V makes it a good classifier (of vegetation) whereas the large scale character makes of W a good quantifier (of water content). This aspect will be dealt with in a quantitative way in Section 4.3.

4. Results and discussion

An assessment on the potential of coordinates V and W to discriminate vegetated surfaces and to be used as a proxy of their water content will be performed by analyzing the set of 16 images that was described in Section 2 (see Table 1). For that purpose a supervised validation of results will be first undertaken by choosing several types of surfaces and by then comparing the respective representations in the η/ξ space with those in the traditional MIR/NIR and R/NIR spaces. This study is then followed by an unsupervised validation that will help evaluating the discriminating ability of V and the sensitivity of W, i.e. the usefulness of V as a classifier and of W as a quantifier. Finally, a quality assessment of the two proposed indices will be undertaken by comparing, for a set of surface types, intra-class and inter-class variability of V and W against the corresponding variability of VI20, BAI20 and GEMI20.

4.1. Supervised validation

As shown in Figs. 12–15 corresponding to scenes 3, 4, 6 and 8, respectively (see Table 1), different classes of surfaces (namely dense vegetation, sparse vegetation, soil, burned vegetation, water, clouds and cloud shadows) were selected by visual inspection of the respective high resolution Landsat ETM + images. The corresponding MODIS data were then used to represent the chosen surfaces in the R/NIR, MIR/NIR and η/ξ spaces. As expected, the representation of the different surfaces in the three spaces are topologically equivalent in the sense that each representation may be continuously transformed into the other by means of translations, rotations and deformations.

Fig. 8. Coordinate lines V = const (from −1 to 1 with intervals of 0.2) and W = const (from 0 to 1 with intervals of 0.2) over the kite domain U'. Coordinate lines were obtained by applying Eqs. (A5) and (A7) over the kite domain U' (see Appendix).
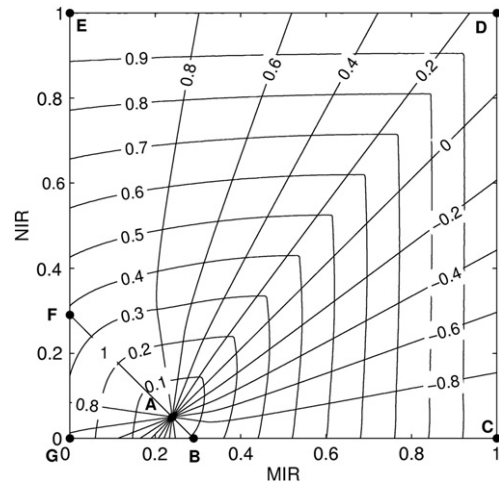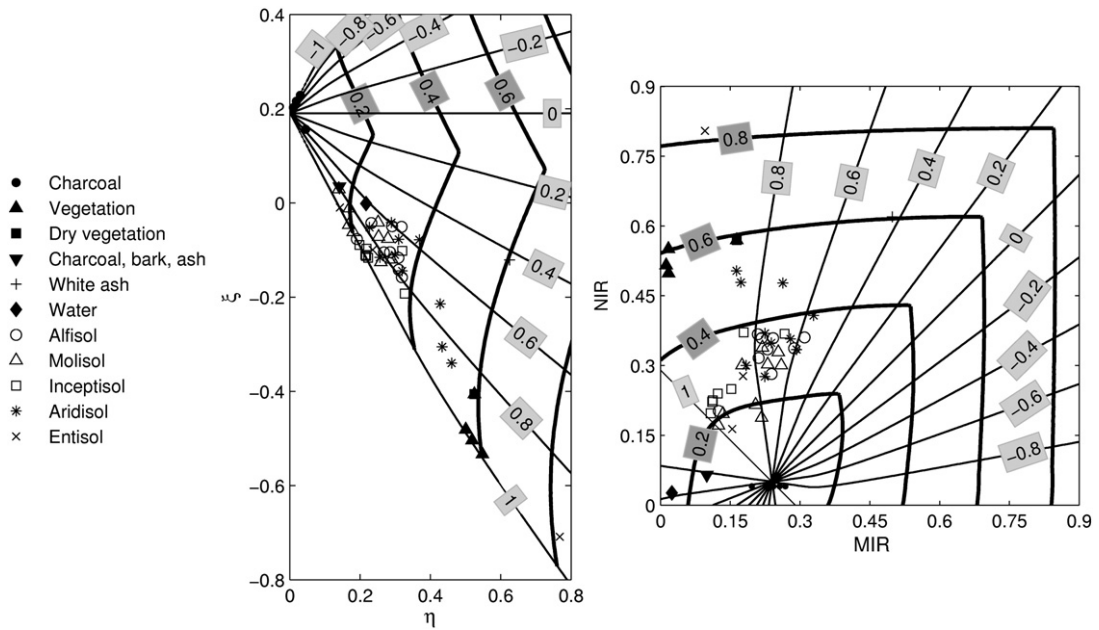
Fig. 10. As in Fig. 6 (left panel) and in Fig. 2 (right panel) but with representation of coordinate curves of V (thin lines) and of W (thick lines) on spaces η/ξ and MIR/NIR, respectively. Laboratory measurements include discrimination among soil types.

The advantages of the η/ξ space together with the associated system of coordinates (V, W) are nevertheless conspicuous. Whereas vegetation, soil and burned pixels tend to lie along the coordinate curve $V = 1$, the position of the remaining pixels is always displaced off the curve. In fact, the trend for surfaces with (without) organic matter to lie close to (away from) $V = 1$ was found in all 16 scenes analyzed, with no exception for any surface. On the other hand, the two extreme values of W are associated with opposite characteristics of vegetated surfaces; whereas burned surfaces tend to have values of W close to zero, especially shortly after the fire event; green vegetation tends to be characterized by high values of W. Intermediate values of W generally correspond to a decreased density of vegetation and/or to the emergence of the soil background.

It may be finally noted that the alignment of vegetated surfaces with the coordinate curve $V = 1$ is mainly due to the already mentioned strict scale character of that coordinate, whereas the large scale character of W allows its usage as a proxy of the water content of vegetated surfaces. It is therefore to be expected that such characteristics will enable the use of coordinates (V, W) to discriminate vegetated surfaces and to grade their water content. This will be investigated in the next subsection.

4.2. Unsupervised validation

The performance of coordinates V and W respectively as a classifier of vegetated surfaces and as a proxy of water content may be assessed
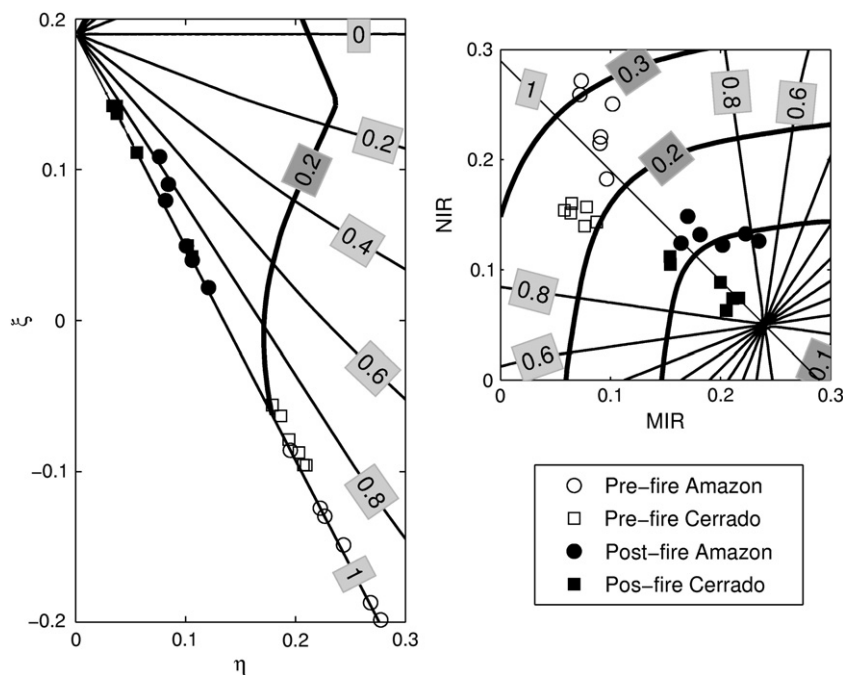

Fig. 11. As in Fig. 10 but respecting to pre- and post-fire pixels as shown in Fig. 7 (left panel) and in Fig. 4 (right panel).
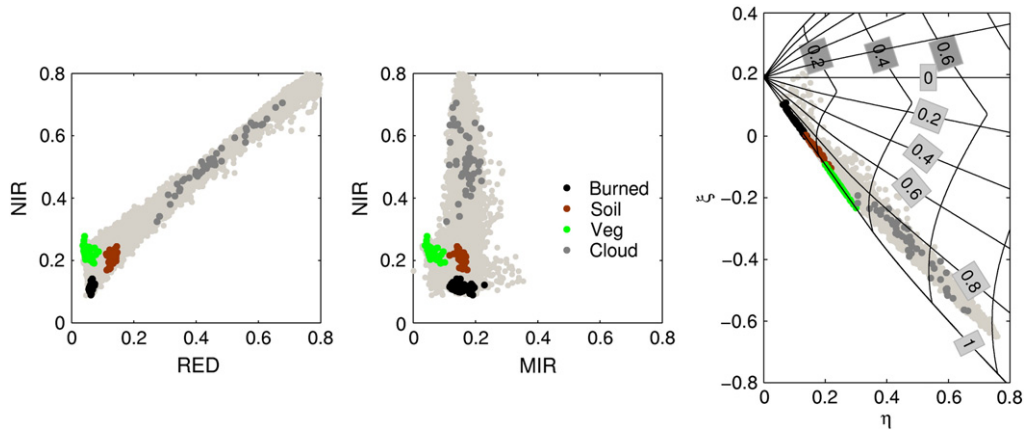
Fig. 12. Scatter plot (light gray dots) of MODIS pixels corresponding to scene 3 in the R/NIR space (left panel), in the MIR/NIR space (middle panel) and in the η/ξ space and respective coordinate lines of V and W (right panel). Selected pixels corresponding to burned surfaces, soil, vegetation and clouds are respectively represented by black, brown, green and gray circles.

by means of an unsupervised technique that allows distinguishing among classes such that the between-group variance of the specified number of classes is maximized. A commonly used unsupervised technique is the one know as K-means or C-means (MacQueen, 1967) which essentially consists in prescribing an initial cluster centre for each of the sought-after clusters and then assigning each pixel of the set to the class nearest to the pixel. A new cluster centre is calculated and pixels are reassigned accordingly. The procedure is repeated until no significant changes in pixel assignments occur from a given iteration to the next.

Taking into account the different characteristics of V and W that make of them respectively a good classifier and a good quantifier, the K-means algorithm was successively applied to coordinates V and W of several MODIS images; i) two cluster centers were estimated from the V sample (respectively associated to vegetated surfaces and to other types) and ii) four clusters were then derived from the W sample restricted to those pixels belonging to the cluster associated to vegetated surfaces (i.e. the one with centre of higher V). Results obtained from the unsupervised classification of each image were finally compared against Landsat ETM + high resolution image taken on the same day (see Table 1).

Figs. 16 and 17 present the results obtained after applying K-means to scenes 3 and 4, respectively. Regarding to the η/ξ space (left panel), gray points correspond to the first of the two clusters obtained by applying K-means to V whereas colored points represent the second cluster. This second cluster was then used as input to a second

K-means procedure which was applied to coordinate W. Thus each colored cluster denotes the clusters derived from the K-means from W, as suggested by the drawn contour lines indicating the limits between these clusters. It is worth noting that colors in the left and central panels correspond to the same clusters. Taking for reference the RGB (543) of the high resolution images (Figs. 16 and 17, right panels), it may be visually confirmed that, when applied to the V samples, the K-means algorithm is able to discriminate between pixels associated to vegetated surfaces (green vegetation, stressed vegetation, and burned surfaces), on the one hand and to the other non-vegetated types (e.g. water bodies and clouds), on the other. The two clusters, whose centres respectively present a high and a low value of V, will be hereafter referred to as vegetated and "other" types. "Other" pixels correspond therefore to the gray points in the left panels of Figs. 16 and 17, whereas the remaining colors identify the pixels belonging to the vegetated type. When K-means is further applied to vegetated pixels, the obtained four clusters in W appear to be related respectively to one class of green vegetation (represented in green), two classes of soil or dry vegetation or sparsely vegetated areas (represented in dark green and dark brown) and one class of burned surfaces (represented in black). A close agreement may be visually identified between the spatial patterns of the above-referred five classes (central panels) and the spatial distribution of RGB (543) pixels (right panels). For instance, the "other" types cluster corresponds to clouds in case of scene number 3 (Fig. 16) and to water in case of scene 4 (Fig. 17); the green vegetation class corresponds to the
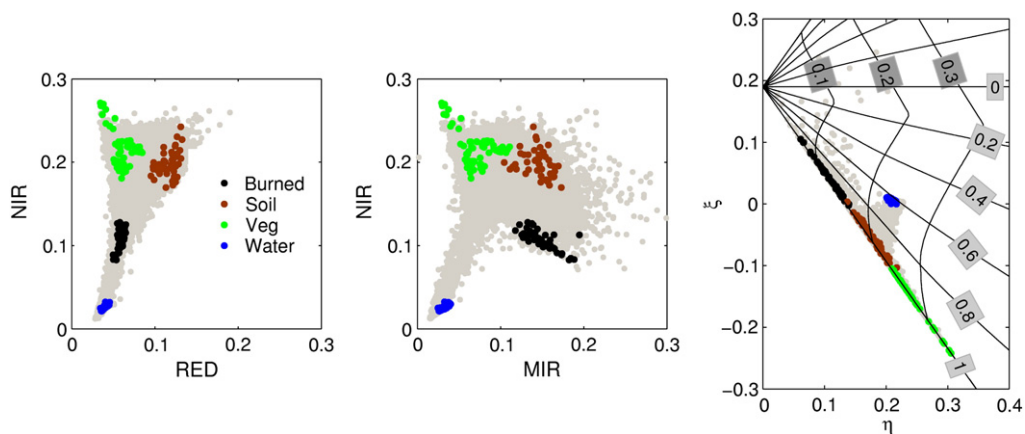

Fig. 13. As in Fig. 12 but respecting to scene 4. Selected pixels representative of burned surfaces, soil, vegetation and water are respectively represented by black, brown, green and blue circles.
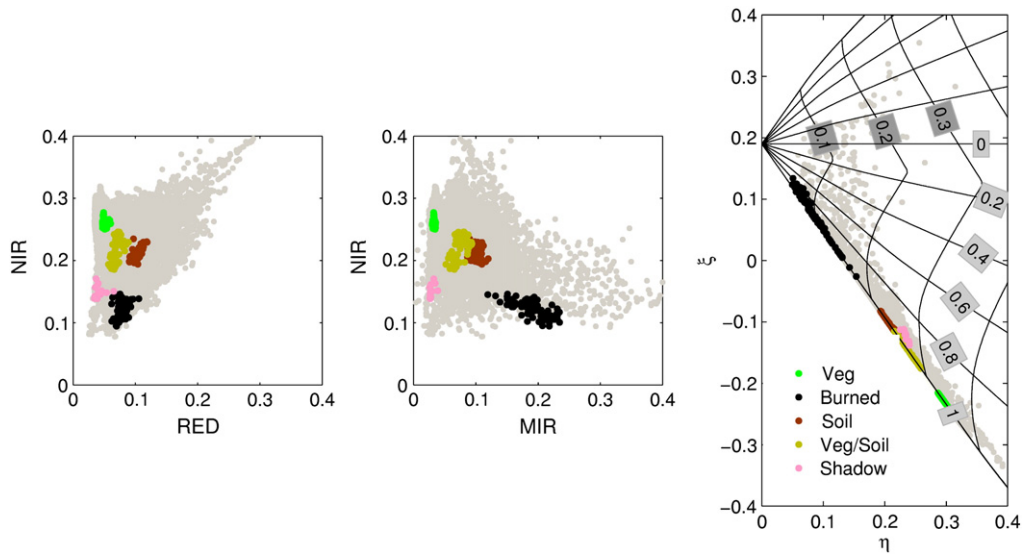
Fig. 14. As in Fig. 12 but respecting to scene 6. Selected pixels corresponding to burned surfaces, soil, vegetation, sparse vegetation and cloud shadows are respectively represented by black, brown, green, olive green and pink circles.

greener patches in both scenes, the soil-stressed/sparse vegetation may be identified as the pinkish and purple areas; finally, the burned surfaces are readily identifiable as the very dark or black pixels of the ETM + images. As expected, in the η/ξ space, the grey pixels (i.e. those belonging to the "other" types cluster do not stand close to coordinate curve V = 1, as opposed to the "vegetated" type cluster, whose pixels lie along that coordinate curve.

A summary of results of K-means for all 16 scenes is presented in Table 4 and the obtained overall consistency is worth being noted. In all 16 scenes analyzed the V cluster with centroid around 0.97 to 0.99 is associated with vegetated surfaces containing. As expected, the other V cluster is less stable, since it considerably depends upon the "other" types of surface (e.g. clouds or water bodies) that is present in the image. The centres of the W clusters also depend on the types of landcover in each scene and, for this reason; results have to be compared against the high resolution image taken on the same day. Accordingly, scenes 1, 2, 3, 4, 5, 6, 7, 10 and 14, that contain burned areas always have the cluster with centre of lowest value (close to 0.1). On the other hand, scenes mostly covered by vegetation, usually

have the cluster with centre of highest value (about 0.23). Finally, soil and sparsely vegetated areas are associated to clusters with centre values between 0.15 and 0.22.

4.3. Quality assessment

Even if obtained on visual grounds, results of the preceding two sections provide evidence about the usefulness of coordinates V and W to discriminate vegetated surfaces and rank them according to the water content (e.g. as green, dry and burned vegetation). The discriminating ability of V and the capacity of W to rank vegetated surfaces in terms of the water contents will now be compared, on a quantitative basis, with those of other currently used indices, such as VI20, BAI20 and GEMI20, which are also based on NIR and MIR information.

Intra-class variability of each index was assessed by means of the corresponding coefficients of variation of each class which are defined as the ratio of the standard deviation to the mean of the respective class. The coefficient of variation is a normalized measure
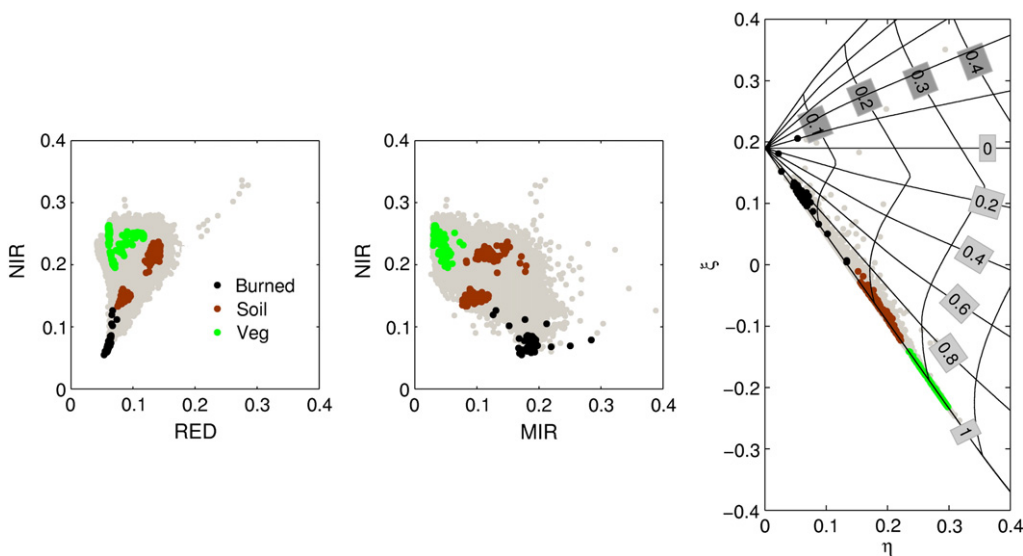

Fig. 15. As in Fig. 12 but corresponding to scene 8. Selected pixels representative of burned surfaces, soil and vegetation are respectively represented by black, brown and green circles.
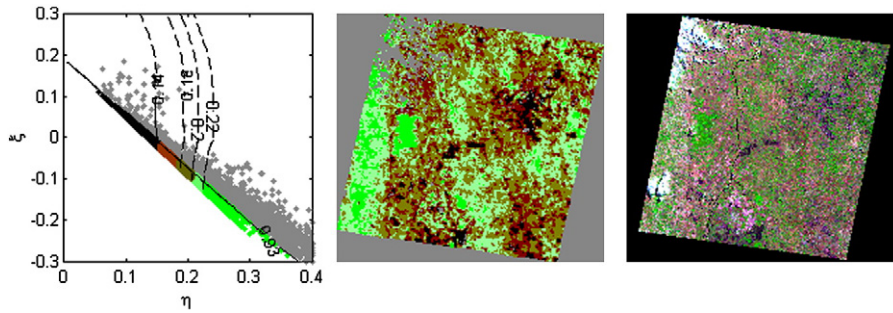
Fig. 16. Comparison of results of K-means corresponding to scene 3 in the η/ξ (left panel) and the geographical (central panel) spaces with the RGB (543) of the corresponding high resolution ETM + image (right panel). See main text for color codes of clusters.
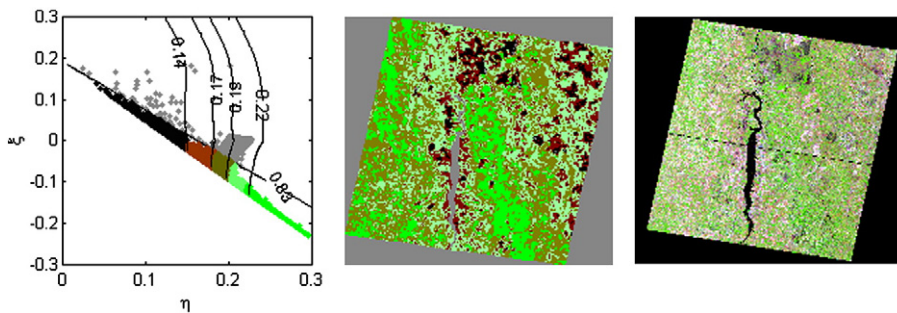

Fig. 17. As in Fig. 16, but corresponding to scene 4.

of dispersion of a given sample and results (Table 5) were obtained for a set of five classes of pixels that were extracted from the above-considered scenes 3, 4, 6 and 8 (see Table 1).

The strict scale character of coordinate V, that was already pointed out, translates into the small values of the coefficients of variance that are the lowest for each type with the exception of clouds where W ranks first. The quite large differences in the values of the coefficient of variation that separate V (for classes where it ranks first) from the corresponding values of the remaining indices (namely VI20 and BAI20) are worth being noted since they provide evidence of the usefulness of V as qualifier, in particular as a discriminator of vegetation, either green or burned, from other types of surface.

Inter-class variability of each index was assessed by means of the discrimination index M as defined in Eq. (6). Coordinate W presents the best discriminating ability respecting to burned vegetation vs. either green vegetation or soil, closely followed by GEMI20 and VI20.

Nevertheless, the result obtained for W is especially relevant since the information provided may be used in conjunction with information from coordinate V that was found to be the best qualifier of vegetated surfaces. The superiority of coordinate V as a qualifier further reflects in the exceptionally high values of M in the case of water vs. green vegetation, burned vegetation and soil.

The potential of using together coordinates V and W may be assessed by noting that, in the case of the coefficient of variation (Table 5) the pair (V, W) leads in all five considered classes (4 for V and 1 for W) and, in the case of the case of the discriminating index M (Table 6) the pair (V, W) leads in seven classes (five for V and 2 for W) out of 10, the remaining three being evenly distributed by GEMI20, BAI20 and VI20. An overview of the performance of all indices in what respects to the intra-class and inter-class variability is provided by the diagrams presented in Fig. 18.

The strict scale character of coordinate V that makes of it a good classifier of vegetated surfaces (either green or burned) translates into the fact that the corresponding quadrilateral is very close to the origin (Fig. 18, left panel) as a result of the very low values of the coefficient of variance for the four considered types of surface. The large scale character of W that allow its usage as a proxy of water content of vegetated surfaces (from green to burned vegetation) is supported by the large area enclosed by the corresponding hexagonal shape which is closely followed by GEMI20. Finally, the complementary character of coordinates V and W reflects in the large differences of the areas

Table 4
Centres of clusters as obtained from applying K-means to coordinates V and W of the 16 scenes described in Table 1.

Scene number	V Cluster centre 1	V Cluster centre 2	W Cluster centre 1	W Cluster centre 2	W Cluster centre 3	W Cluster centre 4
1	0.99	0.77	0.11	0.15	0.17	0.19
2	0.99	0.72	0.14	0.17	0.19	0.20
3	0.99	0.87	0.12	0.16	0.18	0.20
4	0.99	0.66	0.12	0.16	0.18	0.20
5	0.98	0.66	0.14	0.21	0.22	0.24
6	0.99	0.42	0.13	0.20	0.23	0.27
7	0.99	0.49	0.10	0.16	0.20	0.24
8	0.99	0.90	0.16	0.20	0.23	0.27
9	0.99	0.57	0.22	0.25	0.28	0.30
10	0.99	0.51	0.13	0.20	0.24	0.28
11	0.97	0.87	0.23	0.27	0.29	0.31
12	0.99	0.98	0.23	0.28	0.30	0.31
13	0.99	0.97	0.25	0.28	0.31	0.32
14	0.99	0.93	0.14	0.18	0.22	0.26
15	0.99	0.89	0.22	0.24	0.26	0.28
16	0.99	0.84	0.21	0.26	0.29	0.46

Table 5
Coefficients of variation for five types of surfaces for coordinates V and W as well as for VI20, BAI20 and GEMI20. Lowest values of coefficient of variation for each class are highlighted in **bold**.

Surface types	Number of pixels	V	W	VI20	BAI20	GEMI20
Green vegetation	343	**0.002**	0.10	0.19	0.23	0.09
Burned vegetation	255	**0.07**	0.29	0.64	1.05	0.40
Soil	391	**0.02**	0.11	0.43	0.26	0.12
Cloud	70	1.50	**0.21**	0.48	1.06	0.31
Water	56	**0.01**	0.02	0.32	0.04	0.03

Table 6
Values of M index for coordinates V and W, and for VI20, BAI20 and GEMI20. Highest values for each pair of classes are highlighted in **bold**.

Surface pairs	V	W	VI20	BAI20	GEMI20
Burned / Green vegetation	0.80	3.32	**3.31**	1.11	3.21
Burned vegetation / Soil	0.35	**2.08**	1.86	0.98	1.83
Burned vegetation / Water	**5.41**	3.81	0.65	1.06	0.02
Burned vegetation / Cloud	0.63	2.93	3.04	1.17	**3.32**
Green Vegetation / Soil	0.92	1.36	**1.49**	1.23	1.34
Green vegetation / Water	**41.0**	2.01	4.90	2.20	6.88
Green vegetation / Cloud	**1.99**	1.48	0.59	1.39	0.89
Soil /Water	**14.8**	0.36	2.41	0.49	3.64
Soil / Cloud	1.34	2.08	1.05	**2.10**	1.88
Water / Cloud	**4.18**	2.44	4.67	4.74	5.73

enclosed by the respective quadrilaterals (Fig. 18, left panel) and hexagonal shapes (Fig. 18, right panel).

5. Concluding remarks

A transformation was defined on the MIR/NIR space of reflectances with the aim of enhancing the spectral information in such a way that vegetated surfaces may be effectively discriminated and then ranked according to the water content of vegetation, leading to the distinction among green vegetation and burned surfaces. The transformation consisted of 1) the distance η of each point in MIR/NIR to a pre-defined convergence point, representative of a given target (e.g. a totally burned surface), and 2) the difference ξ between the respective MIR and NIR reflectance of each point. The transformation was in fact designed to make a synergic use of advantages of indices, like BAI, that rely on the concept of distances to a fixed point and of indices, like NDVI and VI, which incorporate differences between channels.

When the defined transformation was applied to the unit square of reflectance in the MIR/NIR space, the resulting "kite" domain revealed the property that laboratory materials and land surfaces corresponding to green, dry and burned vegetation tended to lie along the bottom boundary line. A coordinate system was therefore defined in the "kite" domain in such a way that the boundaries of the domain were coordinate curves. The proposed coordinate system presented the two following properties; 1) one of the coordinates, the so-called V coordinate, had a very small dispersion for pixels associated to vegetated surfaces (e.g. green vegetation, sparse vegetation, some types of organic soil and incompletely burned surfaces), whereas 2) the other coordinate, the so-called W coordinate, covered a wide range of values allowing its use as a proxy of the water content of

vegetated surfaces. These two properties are extremely convenient for application purposes since, as pointed out by Verstraete and Pinty (1996), the strict scale character of V makes it a good classifier (of vegetated surfaces) whereas the large scale character of W makes it a good quantifier (a proxy of water content). The new coordinate revealed therefore the ability to provide more information than ratio or modified ratio indices (like most vegetation indices), which also rely on a pair of spectral bands.

A validation exercise was performed with the aim of assessing the potential of coordinate V to discriminate vegetated surfaces and of coordinate W to be used as a proxy of their water content. For that purpose a set of 16 scenes were used covering the two main Brazilian biomes, namely the Amazon Forest and the Cerrado region during the year of 2002. Data consisted of information from Landsat ETM + and of MIR radiance, NIR reflectance and TIR brightness temperature as acquired by MODIS instrument.

A supervised validation was first carried out by selecting, in the scenes, different classes of surfaces (namely vegetation, sparse vegetation, soil, burned vegetation, water, clouds and cloud shadows). Results obtained allowed a deeper understanding of the relevant properties of the (V, W) coordinate system. In fact, the representation of the surfaces in the space η/ξ may be viewed as resulting from the MIR/NIR space by means of translations, rotations and deformations leading to a compression in V and a dilation in W that determine the above-mentioned strict scale character of V and large character of W. Vegetated surfaces tended to lie close to and along the coordinate line $V = 1$, whereas the remaining ones, such as clouds, water bodies, mineral soil and completely burned surfaces (i.e. charcoal only) were mainly located away from that contour line. Nevertheless, burned surfaces in MODIS imagery always fell close to $V = 1$ because it is virtually impossible to find a MODIS pixel completely covered by charcoal and without any trace of biomass. On the other hand, values of W from low to high values were associated with different levels of water content, from full coverage of green vegetation, going across sparsely or senescent vegetation up to burned areas, which are very dry.

The robustness of the coordinate system was then tested by using an unsupervised validation approach, where no a priori knowledge was assumed about V and W data. It was shown that even when using a simple unsupervised clustering algorithm, such as K-means, appropriate and consistent clusters could be found in all the 16 scenes in what regards to the biomass/non-biomass character of the surfaces and their water content. It seems therefore reasonable to conclude that the (V, W) coordinate system is especially adequate to discriminate vegetated surfaces and rank them according to the water content (e.g. as green, dry and burned vegetation).
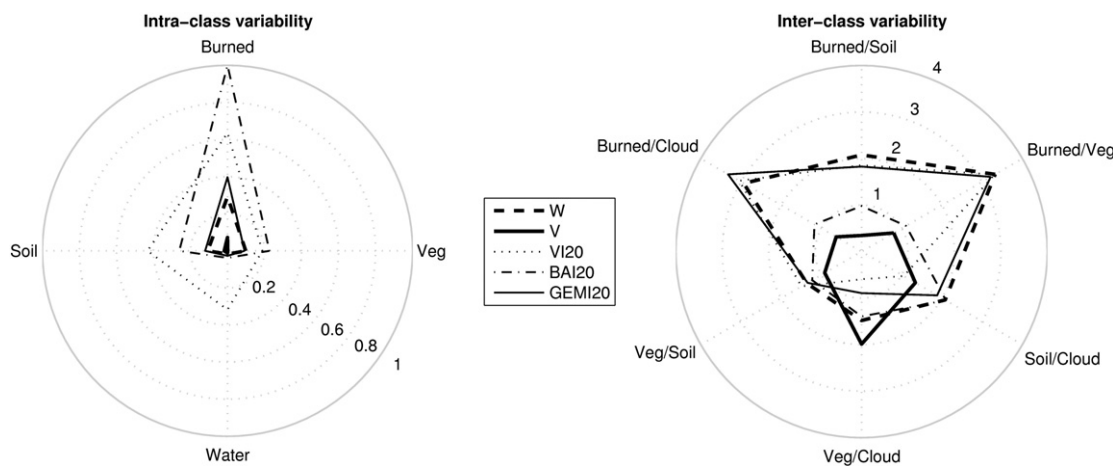

Fig. 18. Overall comparison of intra-class variability for four surface types (left panel) and of inter-class variability for six pairs of surface types (right panel) for coordinates V and W and for GEMI20, VI20 and BAI20.

Performance of the (V, W) coordinate system was finally assessed by comparing, for a selected set of surface types, intra-class and inter-class variability of V and W against the corresponding ones of VI20, BAI20 and GEMI20 which are three commonly used indices also based on MIR and NIR information. The potential of using together coordinates V and W translated into the fact that V had less intra-class variability for four surface types (and W for the remaining one) and that the pair (V, W) showed the largest discriminating ability for seven pairs of classes (five for V and 2 for W) out of 10, the remaining three being evenly distributed by GEMI20, BAI20 and VI20.

The concept behind the (V, W) coordinate system presents some similarities with the tasseled cap transformation, where a new coordinate system is used in order to emphasize vegetation properties. On the other hand, the properties of the η/ξ space and of the associated (V, W) coordinate system open interesting perspectives for applications like drought monitoring and burned area discrimination using remotely-sensed information. The potential of the (V, W) coordinate system to be operationally used to discriminate burned areas in the Amazon and Cerrado regions of Brazil is currently being assessed with very encouraging preliminary results.

Finally, it is worth emphasizing that, although tested with the MODIS sensor, the proposed transformation may be straightforwardly adapted to other sensors, such as the AVHRR, working in the MIR and NIR bands. The approach may be further extended to other combination of bands, e.g. SWIR/NIR according to the purpose of study and to the availability of remotely-sensed information.

Acknowledgments

Appendix

Analytical deduction of the (V, W) system of coordinates.

Let (η, ξ) be the coordinates defined in the kite domain U' (Fig. 5, right panel) by means of the transformation defined by Eqs. (5a) and (5b). Let us define a new coordinate V such that $V \equiv -1$ along the upper border [A'B'C'] of U' and $V \equiv +1$ along the lower border [A'F'E']. Accordingly,

$$\xi = f(V,\eta) = \begin{cases} f_1(V,\eta), & 0 \le \eta \le p(V) \\ f_2(V,\eta), & p(V) \le \eta \le q(V) \end{cases} \quad \text{and} \quad -1 \le V \le +1 \quad \text{(A1)}$$

where $f_1(V,\eta)$, $f_2(V,\eta)$, $p(V)$ and $q(V)$ will have to fulfill the boundary conditions as defined by Eqs. (14) and (15), respectively for $V = -1$ and for $V = +1$. In the case of f_1 and p this may be easily achieved by defining the coordinate curves f_1 as straight lines with slope proportional to V and by assuming that $p(V)$ is the straight line $\eta = mV + b$ such that $\eta = \sqrt{2}y_0$ for $V = -1$ and $\eta = \sqrt{2}x_0$ for $V = +1$. Accordingly:

$$\xi = f_1(V,\eta) = -\sqrt{2}\eta V + (x_0 - y_0) \quad \text{(A2)}$$

and

$$\eta = p(V) = \frac{\sqrt{2}}{2}[(x_0 - y_0)V + (x_0 + y_0)]. \quad \text{(A3)}$$

A similar approach may be used in the case of f_2 leading to:

$$\xi = f_2(V,\eta) = -\left[\sqrt{\eta^2 - \frac{[p(V)]^2}{2}} + \frac{p(V)}{\sqrt{2}}\right]V + x_0 - y_0, \quad \text{(A4)}$$

which fulfills the boundary conditions given by Eqs. (14) and (15), respectively for $V = -1$ and for $V = +1$. Besides, since by construction $f_1[p(V)] = f2[p(V)]$, the condition of continuity of f at each point $p(V)$ is also fulfilled.

Finally, $q(V)$ may be obtained by solving for η the system formed by Eqs. (13a), (13b) and Eq. (A4), i.e. by computing the coordinate η_{max} of the point of intersection of the coordinate curve V with the right boundary curve [E'D'C']. This system may be solved numerically in a straightforward manner by successively halving the interval containing the solution.

Finally, Eq. (A1) may be inverted leading to:

$$V = F(\eta,\xi) = \begin{cases} F_1(\eta,\xi) = -\dfrac{\xi - (x_0 + y_0)}{\sqrt{2}}, & 0 \le \eta \le p(V) \\ F_2(\eta,\xi), & p(V) \le \eta \le q(V) \end{cases} \quad \text{(A5)}$$

where $F_2(\eta,\xi)$ may be again evaluated by successive halving.

The second coordinate, W, will now be defined in such a way that $W \equiv 0$ at point A'$(0, x_0 - y_0)$ and $W \equiv 1$ along the curve [C'D'E']. Let P' be a generic point within the kite domain U' and let V^* be the coordinate curve V that contains P' and intersects the right boundary curve [E'D'C'] at point R'. Coordinate W of point P' will be accordingly given by:

$$W = \frac{\Lambda(V_*, A' \to P')}{\Lambda(V_*, A' \to R')} \quad \text{(A6)}$$

where $\Lambda(V^*, X' \to Y')$ is the arc length, along coordinate curve V^*, from point X' to point Y'.

Finally, taking into account Eqs. (A1), (A2) and (A4), Eq. (A5) may be written as follows:

$$W = \begin{cases} \dfrac{\sqrt{1 + 2V_*^2}\,\eta_{P'}}{\sqrt{1 + 2V_*^2}\,p(V) + \Psi[p(V), \eta_{R'}]}, & \eta_{P'} \le p(V) \\ \dfrac{\sqrt{1 + 2V_*^2}\,\eta_{P'} + \Psi[p(V), \eta_{P'}]}{\sqrt{1 + 2V_*^2}\,p(V) + \Psi[p(V), \eta_{R'}]}, & \eta_{P'} \ge p(V) \end{cases} \quad \text{(A7)}$$

where the integral given by:

$$\Psi[\alpha,\beta] = \int_\alpha^\beta \sqrt{1 + \frac{V_*^2\,[p(V)]^2}{\eta^2 - \frac{[p(V)]^2}{\sqrt{2}}}}\,d\eta \quad \text{(A8)}$$

may be evaluated by gaussian quadrature.

References

Baldridge, A. M., Hook, S. J., Grove, C. I., & Rivera, G. (2009). The ASTER Spectral Library Version 2.0. *Remote Sensing of Environment, 113*, 711–715.

Barbosa, P. M., Gregoire, J. -M., & Pereira, J. M. C. (1999). An algorithm for extracting burned areas from time series of AVHRR GAC data applied at a continental scale. *Remote Sensing of Environment, 69*, 253–263.

Baret, F., Jackquemoud, S., & Hanocq, J. F. (1993). About the soil line concept in remote sensing. *Remote Sensing Reviews, 5*, 281–284.

Boyd, D. S., & Duane, W. J. (2001). Exploring spatial and temporal variation in middle infrared reflectance (at 3.75 mm) measured from the tropical forests of West Africa. *International Journal of Remote Sensing, 22*, 1861–1878.

Boyd, D. S., Foody, G. M., & Curran, P. J. (1999). The relationship between the biomass of Cameroonian tropical forests and radiation reflected in middle infrared wavelengths (3.0–5.0 mm). *International Journal of Remote Sensing, 20*, 1017–1023.

Boyd, D. S., Phipps, P. C., Foody, G. M., & Walsh, R. P. D. (2002). Exploring the utility of NOAA AVHRR middle infrared reflectance to monitor the impacts of ENSO induced

drought stress on Sabah rainforests. *International Journal of Remote Sensing, 23*, 5141—5147.

Boyd, D. S., Wicks, T. E., & Curran, P. J. (2000). Use of middle infrared radiation to estimate leaf area index of a boreal forest. *Tree Physiology, 20*, 755—760.

Briggs, D., & Mounsey, H. (1989). Integrating land resource data into a European geographical information system: Practicalities and problems. *Applied Geography, 9*, 5—20.

Cohen, W. B., Spies, T. A., & Fiorella, M. (1995). Estimating the age and structure of forests in a multi-ownership landscape of western Oregon, U.S.A. *International Journal of Remote Sensing, 16*, 721—746.

Crist, E. P., & Cicone, R. C. (1984). A physically-based transformation of Thematic Mapper data – the TM Tasseled Cap. *IEEE Transactions on Geoscience and Remote Sensing, 22*, 256—263.

Gates, D. M., Keegan, H. J., Schleter, J. C., & Weidner, V. R. (1965). Spectral properties of plants. *Applied Optics, 4*, 11—20.

Goita, K., Royer, A., & Bussiere, N. (1997). Characterization of land surface thermal structure from NOAA-AVHRR data over a Northern ecosystem. *Remote Sensing of Environment, 60*, 282—298.

Holben, B. N., & Shimabukuro, Y. E. (1993). Linear mixture model applied to coarse spatial resolution data from multispectral satellite sensors. *International Journal of Remote Sensing, 14*, 2231—2240.

Huete, A. R. (1988). A soil-adjusted vegetation index (SAVI). *Remote Sensing of Environment, 25*, 53—70.

Kaufman, Y. J., & Remer, L. A. (1994). Detection of forests using MID-IR reflectance: An application for aerosol studies. *IEEE Transactions on Geoscience and Remote Sensing, 32*, 672—683.

Kauth, R. J., & Thomas, G. S. (1976). The tasseled cap - a graphic description of the spectral-temporal development of agricultural crops as seen in Landsat. *Proceedings on the Symposium on Machine Processing of Remotely Sensed Data* (pp. 41—51). Indiana: West Lafayette.

Liang, S. (2004). *Quantitative Remote Sensing of Land Surfaces*. John Wiley and Sons, Inc 534 pages.

Libonati, R., DaCamara, C. C., Pereira, J. M. C., & Peres, L. F. (2010). Retrieving middle-infrared reflectance for burned area mapping in tropical environments using MODIS. *Remote Sensing of Environment, 114*, 831—843.

MacQueen, J. B. (1967). Some methods for classification and analysis of multivariate observations. *Proceedings of 5th Berkeley Symposium on Mathematical Statistics and Probability. Vol. 1 Statistics* (pp. 281—297). University of California Press.

Martín, M. P. (1998). *Cartografía e inventario de incendios forestales en la Península Ibérica a partir de imágenes NOAA–AVHRR Departamento de Geografía.* Alcalá de Henares: Universidad de Alcalá.

Martín, M. P., & Chuvieco, E. (2001). Propuesta de un nuevo índice para cartografía de áreas quemadas: aplicación a imágenes NOAA-AVHRR y Landsat-TM. *Revista de Teledetección, 16*, 57—64.

MODIS Characterization Support Team — MCST (2006). MODIS Level 1B Product User's Guide : NASA/Goddard Space Flight Center. available at http://www.mcst.ssai.biz/mcstweb/documents/M1054.pdf

Pereira, J. M. C. (1999). A comparative evaluation of NOAA/AVHRR vegetation indices for burned surface detection and mapping. *IEEE Transactions on Geoscience and Remote Sensing, 37*(1), 217—226.

Pinty, B., Lavergne, T., Widlowski, J. -L., Gobron, N., & Verstraete, M. M. (2008). On the need to observe vegetation canopies in the near-infrared to estimate visible light absorption. *Remote Sensing of Environment, 113*(1), 10—23.

Pinty, B., & Verstraete, M. M. (1992). GEMI A nonlinear index to monitor global vegetation from satellites. *Vegetatio, 101*, 15—20.

Richardson, A. J., & Wiegand, C. L. (1977). Distinguishing vegetation from soil background information. *Photogrammetric Engineering and Remote Sensing, 43*, 1541—1552.

Rondeaux, G., Steven, M., & Baret, F. (1996). Optimization of soil-adjusted vegetation indices. *Remote Sensing of Environment, 55*, 95—107.

Rouse, J. W., Haas, R. H., Schell, J. A., & Deering, D. W. (1973). Monitoring vegetation systems in the Great Plains with ERTS. *Third ERTS Symposium, NASA SP-351 I* (pp. 309—317).

Roy, D. P., Giglio, L., Kendall, J. D., & Justice, C. O. (1999). Multi-temporal active-fire based burn scar detection algorithm. *International Journal of Remote Sensing, 20*, 1031—1038.

Salisbury, J. W., & D'Aria, D. M. (1994). Emissivity of terrestrial materials in the 3–5 μm atmospheric window. *Remote Sensing of Environment, 47*, 345—361.

Shimabukuro, Y. E., Holben, B. N., & Tucker, C. J. (1994). Fraction images derived from NOAA AVHRR data for studying the deforestation in the Brazilian Amazon. *International Journal of Remote Sensing, 15*, 517—520.

Slaton, M. R., Hunt, E. R., Jr., & William, K. S. (2001). Estimating near-infrared leaf reflectance from leaf structural characteristics. *American Journal of Botany, 88*, 278—284.

Verstraete, M. M., & Pinty, B. (1996). Designing optimal spectral indices for remote sensing applications. *IEEE Transactions on Geoscience and Remote Sensing, 34*(5), 1254—1265.